THE JOURNAL OF PHYSICAL CHEMISTRY C

Article

pubs.acs.org/JPCC

Chemical Effects of Tin Oxide Nanoparticles in Polymer Electrolytes-Based Dye-Sensitized Solar Cells

Hwaseok Chae,[†,§] Donghoon Song,[†,§] Yong-Gun Lee,[†] Taewook Son,[†] Woohyung Cho,[†] Yong Bum Pyun,[†] Tea-Yon Kim,[†] Jung Hyun Lee,[†] Francisco Fabregat-Santiago,[‡] Juan Bisquert,[‡] and Yong Soo Kang*[,†]

[†]Department of Energy Engineering and Center for Next Generation Dye-sensitized Solar Cells, Hanyang University, Seoul 133-791, Korea

[‡]Photovoltaic and Optoelectronic Devices Group, Department de Física, Universitat Jaume I, 12071 Castelló, Spain

Supporting Information

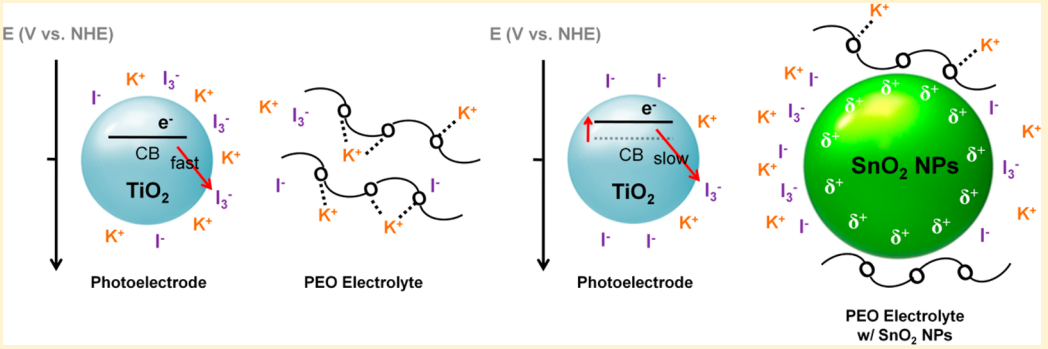

ABSTRACT: The effects on the photovoltaic performance of the incorporation of SnO_2 nanoparticles into the polymer of a solid-state dye-sensitized solar cell (DSC) based on the poly(ethylene oxide)/poly(ethylene glycol) dimethyl ether solid electrolyte are studied in this paper. It has been found that the addition of SnO_2 nanoparticles to the solid electrolyte produces several key changes in the properties of the solid-state DSC that produced a better performance of the device. Therefore, we have measured an improvement in electrolyte conductivity by a factor of 2, a linear rise in the TiO_2 conduction band position, a reduction in the electron recombination rate, and a decrease in charge-transfer resistance at the counterelectrode/electrolyte interface. All these improvements produced an increase in the power conversion efficiency from 4.5 to 5.3% at 1 sun condition, a consequence of the increase of both V_{oc} (oc = open circuit) and J_{sc} (sc = short circuit) without any sacrifice in FF (fill factor). The origin of these changes has been associated to the strong Lewis acidic character of SnO_2 nanoparticles yielding to the formation of a I_3^- percolation layer for holes at the surface of SnO_2 and the reduction of the concentration of free I_3^- and K^+ ions inside the pores of TiO_2. From these results, it is concluded that the physicochemical effects of inorganic nanofiller in the polymer electrolyte may also be considered a good route in designing the high efficiency solid-state DSCs employing the polymer electrolyte.

INTRODUCTION

Since the development of dye-sensitized solar cells (DSCs), they have received great attention as a promising technology as a low cost energy source of the next photovoltaic generation.[1] High energy conversion efficiency of over 12% has been reported for DSCs using a cobalt redox-based liquid electrolyte.[2] However, the liquid electrolyte in DSCs has drawbacks, mostly stemming from solvent evaporation or leakage problems. Many academic studies have been focused on solid-state or quasi-solid-state alternatives utilizing hole transport materials,[4−8] gel and solid polymer electrolytes.[9−17] DSCs using a solid polymer electrolyte have many advantages associated with a solvent-free device such as improved thermal and long-term stabilities, higher environmental safety under breakage of the device, and so forth.

However, the use of solid polymer electrolyte, most commonly with poly(ethylene oxide) (PEO), has some drawbacks that make them less efficient than their liquid counterparts. The most important drawback is the low ionic conductivity, in the range from 10^{-7} to 10^{-5} S cm^{-1} at room temperature, and the low penetration of the PEO into the nanoporous titania electrode, which results in the insufficient utilization of dyes due to the poor interfacial contact between dyes adsorbed TiO_2 surface and the solid polymer electrolyte.[18]

Special Issue: Michael Grätzel Festschrift

Received: November 29, 2013
Revised: February 11, 2014

   dx.doi.org/10.1021/jp4117485 | J. Phys. Chem. C XXXX, XXX, XXX−XXX

There have been several approaches to overcome the limitations associated with the use of solid polymer electrolytes.[9,19−22] One interesting option is to utilize oligomeric poly(ethylene glycol) dimethyl ether (PEGDME) ($M_W \sim 500-1000$) either blended with PEO or nanoparticles (NPs).[21] The blend of PEO and PEGDME enhances the ionic mobility as well as the interfacial contact between dye molecules and electrolyte, thanks to the improvement of pore-filling of the reformulated polymer electrolyte into the mesopores of titania layer in DSCs.[22]

When inorganic NPs are incorporated in polymer electrolyte, both ionic conductivity and mechanical strength are improved.[24,25] They a have large surface area which contains cross-linking centers for the PEO segments, resulting in an increased amorphous region and mechanical strength. The polymer chains separated by the nanofillers are arranged in a three-dimensional and mechanically stable network that creates free volume through which I^-/I_3^- can diffuse, thereby increasing its mobility and consequently its ionic conductivity.[25−27] Many groups have therefore attempted to use NPs such as titanium oxide (TiO_2), silicon oxide (SiO_2), aluminum oxide (Al_2O_3), among others, in polymer and gel electrolytes, eventually to increase the power conversion efficiency of solid-state DSCs.[21,24−29] The increase in the power conversion efficiency by the incorporation of inorganic NPs has been mostly explained by physical effects (without chemical effects) such as the increase in the ionic conductivity due to the decrease in the crystallinity of polymer matrix used and the increase in the interfacial free volume between NPs and polymer matrix.

Inorganic NPs show different Lewis-acidity or -basicity depending on their chemical structure. For instance, tin oxide (SnO_2) is a stronger Lewis acidic relative to TiO_2.[30] The acidity of the inorganic NPs dispersed in a polymeric matrix may affect the photovoltaic behavior of DSCs. In this work, strong (Lewis) acidic SnO_2 NPs are introduced into PEO/PEGDME polymer electrolytes to investigate both their physicochemical effects on the electrolyte and on the power conversion efficiency of DSCs. In particular, chemical interactions of the inherently partially positively charged acidic property of SnO_2 NPs[30] with anions such as I^- and I_3^- and lone pairs of oxygen of PEO chains will be investigated.

EXPERIMENTAL SECTION

Materials. Poly(ethylene oxide) (PEO, M_w = 1 000 000 g/mol), poly(ethylene glycol) dimethyl ether (PEGDME, M_w = 500 g/mol), potassium iodide (KI), iodine (I_2), and tin oxide (SnO_2, <100 nm) NPs were purchased from Sigma Aldrich. Acetonitrile (AN) to dissolve the salts was purchased from Wako. Fluorine doped tin oxide (FTO)-coated conductive glass substrates (TEC-8) with a sheet resistance of 8 Ω/square were purchased from Pilkington. Transparent titania nanoparticulate paste (TiO_2 PASTE DSL 18NR-T) was purchased from Dyesol, and *cis*-diisothiocyanato-bis (2,2′-bipyridyl-4,4′-dicarboxylato) ruthenium(II) bis (tetrabutylammonium) (Ruthenizer 535 bis-TBA, also known as N719) was received from Solaronix. All chemicals were reagent grade and were used as received without further purification.

Preparation of Polymer Electrolytes. Polymer electrolytes were prepared by the blend of PEO (M_W= 1 000 000 g/mol) and PEGDME (M_W = 500 g/mol) with a mole ratio of [−O−]:[KI]:[I_2] = 10:1:0.1, and the ratio of PEO and PEGDME was fixed at 4:6 (w/w). Further details are described in our previous paper.[23] The SnO_2 (<100 nm) NPs were added and dispersed in the PEO/PEGDME polymer electrolytes. The amounts were 5, 10, and 15 wt % of the total polymer electrolyte. After the SnO_2 NPs were fully dispersed, the highly viscous electrolytes were dried overnight in an oven (40 °C) to remove traces of solvent.

Fabrication of DSCs. The FTO glass substrates were cleaned with a detergent solution in an ultrasonic bath for 20 min, followed by cleaning in DI water and ethanol for 15 min each. These FTO glasses were used for both working and counter electrodes. For preparing the working electrodes, a blocking layer of TiO_2 films was spread on the FTO glass surface by spin-coating 2 wt % of Ti(IV) bis(ethyl acetoacetato)-diisopropoxide in 1-butanol solution and sintered at 450 °C for 30 min. Thin-nanostructured TiO_2 film was prepared from ∼20 nm NPs by the doctor-blade technique on conductive glass substrates, followed by heating at 450 °C for 30 min. The thickness of the transparent electrode was approximately 6−7 μm, and the active area of the cell was fixed to 0.25 cm^2 to allow for consistent measurements of power conversion efficiency under illumination, respectively. The TiO_2 electrodes were subsequently dipped into 0.5 mM N719 dye in an AN/*tert*-butanol solvent (1:1, v/v) for 18 h at 30 °C. Then, the dye-sensitized TiO_2 film was rinsed with the AN and dried in the dark. Counter electrodes were prepared by spin coating 0.01 M H_2PtCl_6 solution onto FTO glass, followed by sintering at 450 °C for 30 min. Surlyn (25 μm, Dupont) was attached to the photoelectrodes as a spacer, and polymer electrolyte was casted onto working electrode. Finally, the two electrodes were subsequently clipped together, and the cells were stored in an oven (40 °C) for the evaporation of retained solvent.

Characterization. The macroscopic structure and crystallinity of polymer electrolyte was examined by X-ray diffraction (XRD) in the range of ∼10−50°, which was performed at room temperature using a high-resolution X-ray diffractometer (Rigaku, D/MAX-2500/PC). The ionic conductivities of the bulk polymer electrolyte were measured with an IM6 potentiostat (Zahner). To analyze the transport behavior of I_3^- in polymer electrolyte, linear sweep voltammetry (LSV) was measured by an Autolab instrument in the potential cycled range from −0.5 to 0.5 V at the scan rate of 5 mV/s. UV−vis absorption spectra were monitored with JASCO/V-670 spectrophotometer to analyze the light absorption of I^-/I_3^- redox. Reflectance spectra were obtained with the spectrophotometer equipped with a spherical accessory. The photocurrent−voltage (J−V) characteristics were carried out using a solar simulator, with a 300 W xenon arc-lamp (Newport) under 1 sun illumination (AM 1.5, 100 mW/cm^2). The intensity of light illumination was calibrated by a silicon solar cell (PV Measurements, Inc.). The J−V data were recorded with a shading mask to avoid the overvaluation of power conversion efficiency. The incident photon to current conversion efficiency (IPCE) of DSCs was measured by QEX7 (PV Measurements, Inc.). Electrochemical impedance spectroscopy (EIS) using an IM6 (Zahner) was used to investigate the interfacial properties between counter electrode and electrolyte in the frequency range of 1 MHz to 500 mHz at cell voltage E = 0 V under dark condition. The electron lifetime, electron diffusion coefficient, and trapped charges in TiO_2 films in DSCs were evaluated from methods of intensity-modulated photovoltage spectroscopy (IMVS), intensity-modulated photocurrent spectroscopy (IMPS), and charge extraction (CE) (CIMPS-abs, Zahner).

dx.doi.org/10.1021/jp4117485 | J. Phys. Chem. C XXXX, XXX, XXX−XXX

RESULTS AND DISCUSSION

Interaction of SnO_2 with Lewis Bases in the Polymer Electrolyte. Strong Lewis acidity of SnO_2 NPs could make their surface positive, and therefore, they could interact with Lewis base such as I^-, I_3^-, and ethylene oxide units in the PEO-based polymer electrolyte. The relative acidity scale of SnO_2 is quantitatively represented by 3.473, whereas TiO_2 is 3.046.[30] Note that the larger value indicates an increased acidity.

Because the acidity of SnO_2 NPs is increased compared to that of TiO_2, the I^- and I_3^- ions will be preferentially adsorbed on the surface of the SnO_2 NPs, as illustrated in Figure 1. To

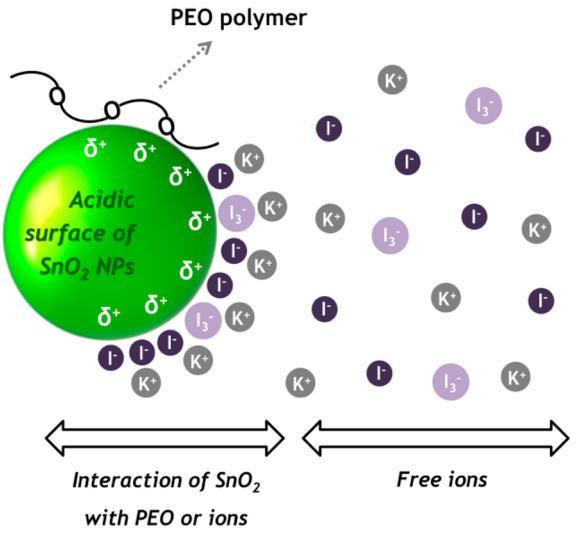

Figure 1. Schematic formation of the discrete anion-rich layer and an improved contact with ethylene oxide units of PEO due to the interactions between the acidic surface of SnO_2 and basic ions (I_3^- and I^-) and oxygens from electrolyte.

determine the amount of I_3^- adsorption onto the SnO_2 surface, we prepared one electrolyte based on oligomeric liquid PEGDME only. The composition of the prepared electrolyte is fixed at [−O−]:[KI]:[I_2] = 10:1:0.1 (O is from PEGDME only) with or without the SnO_2 NPs. After a centrifugal and settling-down process, the upper solution part was separated, followed by a 100-fold dilution. The UV−vis absorption spectra of these dilutions are depicted in Figure 2. The addition of SnO_2 diminished the absorbance peak intensity at around 370 nm, thereby indicating that the I_3^- concentration is larger in the SnO_2 free solution. From data in Figure 2, we could estimate that 20% of I_3^- was adsorbed on the acidic surface of SnO_2.

In general, the PEO-segmental motion in the neat PEO polymer is significantly restricted due to the presence of many crystallites, resulting in a low ionic conductivity. It is therefore important to reduce its crystallinity for the improvement in the ionic conductivity.[18] Upon incorporating SnO_2 into PEO/PEGDME without any salts, the crystallinity of the polymer was reduced markedly as evidenced by XRD data in Figure 3. The peaks of crystalline PEO at 2θ = 19.1° and 23.3° are assigned as (120) and (112), mirroring the presence of PEO crystals, and the peaks at 2θ = 27°, 34° and 38° correspond to the SnO_2 NPs crystals.[31] These results suggest that acidic SnO_2 NPs interact also with basic ethylene oxide units of PEO (Figure 1). Moreover, these interactions could induce a three-dimensional and mechanically stable network without phase separation. The PEO/PEGDME crystallinity was also reduced to a large extent

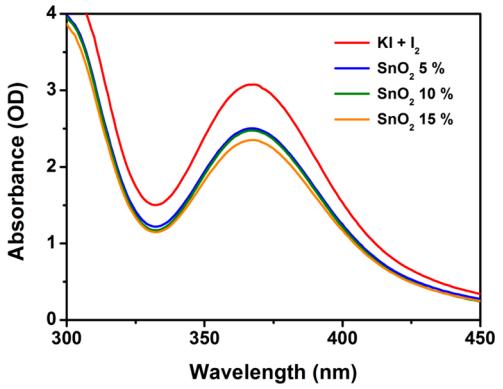

Figure 2. UV−vis absorption spectra of electrolyte solutions containing I^-/I_3^- redox couple with varying the amount of SnO_2 NPs added. The electrolyte composition was [−O−]:[KI]:[I_2] = 10:1:0.1 (O is from PEGDME) with SnO_2 NPs contents (5, 10, 15 wt %).

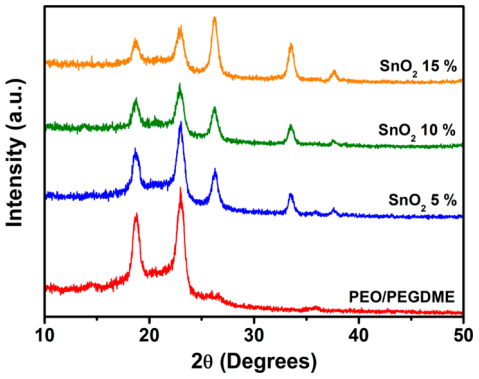

Figure 3. XRD patterns of pure PEO/PEGDME with the amount of SnO_2. Two peaks at 2θ = 19.1° and 23.3° reflect the crystalline of PEO/PEGDME, and the peaks at 2θ = 27°, 34°, and 38° correspond to the (110), (101), and (200) planes of crystalline SnO_2.

by the addition of K^+ ions (Figure S1, Supporting Information), which is consistent with previous reports.[32] However, K^+ ions are well-known to be coordinated by the ethylene oxide units of the PEO chains, which may lose their segmental mobility.

Ionic Transport in Polymer Electrolyte. The ionic transport mainly occurs through amorphous domains but not through crystals of PEO. Upon incorporation of SnO_2 NPs, the PEO chains rearrange in a three-dimensional and mechanically stable network, resulting in an increased amorphous region as described previously. In addition, these interactions may help to increase the free volume at the interphase between SnO_2 NPs and the PEO/PEGDME matrix, improving ionic transport.[33] Moreover, the SnO_2 NPs surrounded by iodide species (I^- and I_3^-) might create percolation paths facilitating the ionic transport.[34]

Figure 4a provides the ionic conductivity (σ) through the polymer electrolyte as a function of the SnO_2 NPs concentrations, measured under ambient conditions from the ac impedance method using the following equation:[35]

$$\sigma = \frac{l}{AR_b} \quad (1)$$

where σ is the ionic conductivity (S/cm), l the length (cm) of the electrolyte, A the surface area of the electrode (cm^2), and R_b the electrolyte resistance (Ω or S^{-1}). The ionic conductivity

dx.doi.org/10.1021/jp4117485 | J. Phys. Chem. C XXXX, XXX, XXX−XXX

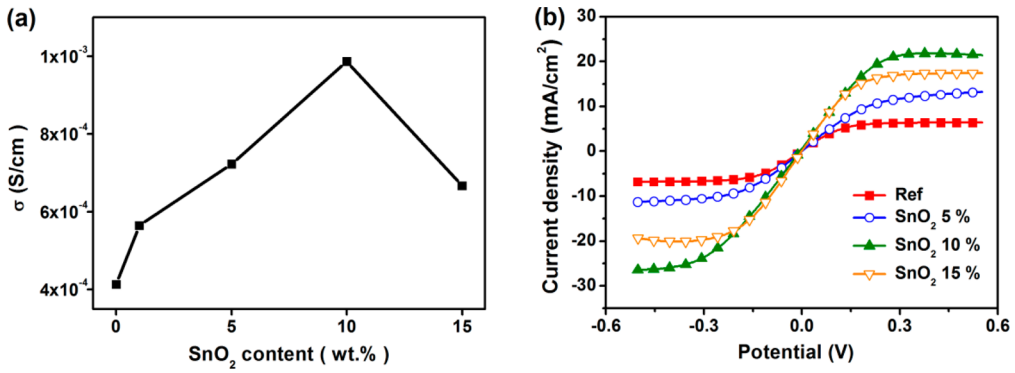

Figure 4. (a) Ionic conductivity for polymer electrolyte at room temperature and (b) linear sweep voltammograms for the Pt−Pt symmetric cells with the cell separation of 25 μm filled with polymer electrolyte containing various amounts of SnO_2 NPs. Scan rate is 5 mV s^{-1}.

was increased with the SnO_2 content and reached the maximum value of 9.87 × 10^{-4} S/cm at 10 wt % of SnO_2 NPs, which is more than twice the value of the SnO_2 free electrolyte. However, the excess addition (15 wt %) of SnO_2 NPs rather decreased the ionic conductivity, presumably due to the phase separation between SnO_2 and the PEO/PEGDME matrix, which will hinder the segmental motion of PEO polymer chains.

To understand the increase in the ionic conductivity upon addition of SnO_2, the diffusion coefficient of I_3^- in the polymer electrolyte was measured by linear sweep voltammetry (LSV) in the potential range of −0.5 to 0.5 V at the scan rate of 5 mV/s (Figure 4b). The diffusion coefficients (D_{app}) of I_3^- in polymer electrolyte were determined by measuring the limiting current density J_{lim} within the electrochemical cells according to the following equation:[36]

$$D_{app} = \frac{d}{2nFC_o} J_{lim} \quad (2)$$

where n = 2 is the electron transfer number required for the reduction of I_3^- to I^-, C_o the bulk concentration of the I_3^-, d the thickness of the cell, and F the Faraday constant. Figure 4b shows that the values of D_{app} (I_3^-) for the polymer electrolyte containing the SnO_2 are higher than that without SnO_2. The polymer electrolyte with 10 wt % SnO_2 showed the highest D_{app} (I_3^-) value (2.77 × 10^{-6} cm^2 s^{-1}) among them, which is around 3 times larger than the value obtained for the NPs free electrolyte. The D_{app} (I_3^-) data show a similar trend with those of ionic conductivity. It is meaningful to note that the addition of 10 wt % SnO_2 NPs in the polymer electrolyte could enhance the I_3^- diffusion as well as the ionic conductivity.

To evaluate how much the SnO_2 NPs could contribute to the I_3^- diffusion in practical operation of DSCs, we measured the photocurrent transient, a well-known tool to trace the I_3^- diffusion transient, and depicted this in Figure 5. The photocurrent decay for the reference cell during the initial 10 s of light exposure indicates a diffusion limitation. This decay is attenuated in all cases in SnO_2 NPs-based DSCs. SnO_2 NPs (10 wt %) induce the least photocurrent decay, indicating that the relatively faster dye regeneration occurs in 10 wt % SnO_2 NPs-based DSC, in good agreement with the previous results of the ionic conductivity and the diffusion coefficient of I_3^- through the solid polymer electrolytes.

Photovoltaic Performance. Figure 6a,b shows the J−V curves of DSCs employing the solid polymer electrolyte by varying the SnO_2 content, under 1 sun illumination (AM 1.5,

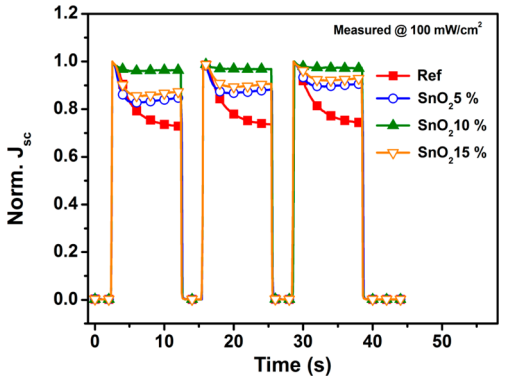

Figure 5. Photocurrent transients of DSCs as a function of the concentration of SnO_2 NPs in polymer electrolytes measured after 10 min under illumination condition.

100 mW/cm^2) and in the dark condition, respectively. The photovoltaic parameters such as open-circuit voltage V_{oc}, short-circuit current J_{sc}, and fill factor FF in Figure 6a are summarized in Table 1. Note that the solid polymer electrolyte DSCs with SnO_2 display both improved V_{oc} and J_{sc} and comparable or slightly increased FF compared to the reference. Specifically, V_{oc} is gradually improved up to 15 wt % SnO_2 and J_{sc} up to 10 wt % SnO_2. As previously remarked, the addition of SnO_2 above 15 wt % derives phase separation, rendering slow I_3^- diffusion and consequently decreasing J_{SC}. The overall power conversion efficiency of 5.33% obtained using 10 wt % SnO_2 outperforms that without SnO_2 NPs (4.47%).

Figure 6b is indicative of the fact that the dark current diminishes with increasing SnO_2 amount in the polymer electrolyte, resulting in the increase in V_{oc} in SnO_2 NPs-based DSCs.

Increase in V_{oc} upon SnO_2 Incorporation: Conduction Band Edge Shift of TiO_2. The open-circuit voltage V_{oc} is defined by the gap between TiO_2 Fermi level and redox potential.[37,38] In other words, at a given redox energy level, the movement of the Fermi level of the TiO_2 electrode arising from the concentration of photogenerated electrons in the TiO_2 determines the observed V_{oc}. The TiO_2 CB position and the electron recombination rate have been reported to be the main factors determining V_{oc} for a given system.[39]

The CB shift depends among others on the net number of negative or positive charges built up on the surface of the TiO_2 layer. This movement affects the distribution of electron states in the TiO_2 and consequently the equilibrium Fermi level and V_{oc}. In particular, the accumulation of positively charged K^+

dx.doi.org/10.1021/jp4117485 | J. Phys. Chem. C XXXX, XXX, XXX−XXX

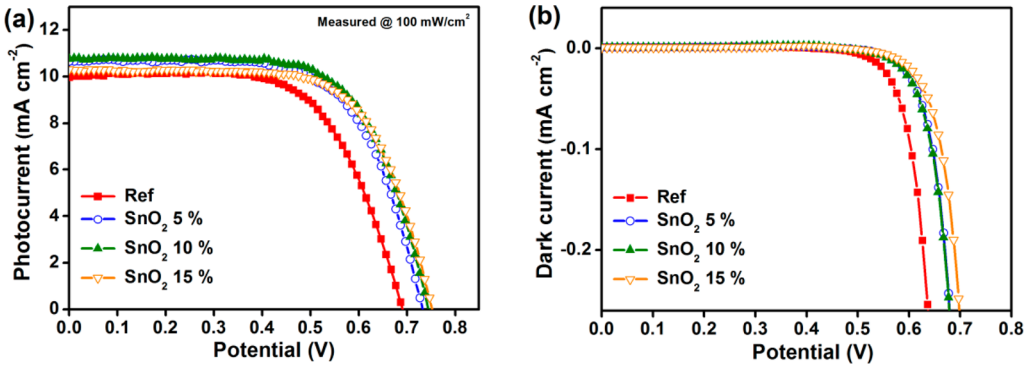

Figure 6. J–V characteristics of DSCs based on polymer electrolytes containing various amount of SnO_2 NPs (a) under 1 sun illumination (AM 1.5, 100 mW/cm^2) and (b) in the dark condition. Active area of devices was 0.25 cm^2 shaded with a 0.25 cm^2 metal mask.

Table 1. Ionic Conductivity (σ), Diffusion Coefficients of I_3^- ($D_{app}(I_3^-)$), and Photovoltaic Performances[a] of DSCs Fabricated by Varying SnO_2 NPs in the Polymer Electrolyte

electrolytes	σ (10^{-4} S/cm)	D_{app} (I_3^-) (10^{-6} cm^2/s)	V_{oc} (V)	J_{sc} (mA/cm^2)	FF	η (%)
ref	4.13	0.81	0.69	10.0	0.65	4.5
SnO_2 5%	7.23	1.66	0.73	10.6	0.66	5.1
SnO_2 10%	9.87	2.77	0.74	10.8	0.66	5.3
SnO_2 15%	6.67	2.21	0.75	10.3	0.67	5.2

[a]V_{oc}: open-circuit voltage; J_{sc}: short-circuit current; FF: fill factor; and η: power conversion efficiency.

from the electrolyte will cause the TiO_2 CB to shift downward. The CB shift is determined by recording, through the charge extraction (CE) method, the relation between the accumulated charge Q_e and V_{oc}, as shown in Figure 7.[40] Note that Q_e

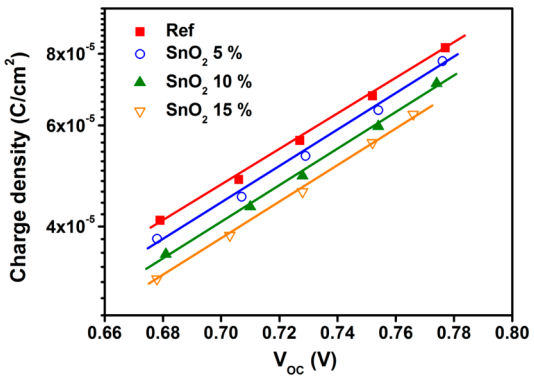

Figure 7. Photoinduced charge density versus open-circuit voltage (V_{oc}) upon the addition of SnO_2 in polymer electrolyte.

decreases at a fixed V_{oc} with the addition of SnO_2 in the polymer electrolyte. Meanwhile, referring to the trap/detrap electron transport, the upward TiO_2 CB shift requires the high energy for the electron detrapping process, slowing down electron diffusion. In other words, electron transport will be another clue of reflecting the CB shift. As shown in Figure S2 in the Supporting Information, at a given photocurrent, the electron diffusion coefficient is gradually reduced with increasing SnO_2.

It is well-known that K^+ ions dissolved in the electrolyte can be adsorbed onto TiO_2 layer, leading to downward CB shift, i.e. decrease in Fermi level. As well, we suspected that the SnO_2 NPs themselves having strong Lewis acidity might be adsorbed onto the TiO_2 layer, shifting the TiO_2 CB too. The ultraviolet photoelectron spectroscopy (UPS) is therefore measured to determine the dominant one between K^+ ions and SnO_2 NPs affecting on the TiO_2 CB level. As evidenced in Figure S3, work function, energy gap between vacuum level and Fermi level, have changed from 5.23 to 5.41 eV by the presence of KI, whereas SnO_2 NPs rarely affect on the TiO_2 CB level. Plausible reasons could be that the SnO_2 used in this work is too large in size (<100 nm) to penetrate and to contact onto TiO_2 layer and also that only point contacts at the surface of the mesoporous layer would be possible among circular TiO_2 and SnO_2 NPs. The upward CB shift of TiO_2 observed with increasing SnO_2 NPs in the electrolyte may then be an indication of a lower amount of adsorbed K^+ ions at the TiO_2 surface. This fact may occur if K^+ ions are accumulated near the anion-adsorbed SnO_2 nanoparticles, as a result of the establishment of the charge neutrality near the interface. As consequence overall free K^+ concentration would be reduced from electrolyte and TiO_2 surface.

Increase in V_{oc} upon SnO_2 Incorporation: Electron Recombination. The concentration of photogenerated electrons in the TiO_2 CB and thereby V_{oc} are also seriously affected by their loss through the interfacial reaction between photoelectrons in TiO_2 layer and I_3^- in the electrolyte (i.e., electron recombination). The recombination follows the relation:

$$j_{rec} \alpha k_r n[I_3^-] \quad (3)$$

with j_{rec} being the recombination current, k_r recombination rate constant, n electron concentration in TiO_2, and $[I_3^-]$ concentration of I_3^- species in electrolyte in contact with TiO_2. Herein, the recombination reaction is characterized by electron lifetimes measured by the IMVS method. The data obtained from the IMVS are expressed by electron lifetime (τ_n) depending on open-circuit potential. To compare the recombination reaction at a similar number of electrons in TiO_2 CB, we use following relation[41,42]

$$V_{ecb} = V_{oc} - \Delta E_C/q \quad (4)$$

dx.doi.org/10.1021/jp4117485 | J. Phys. Chem. C XXXX, XXX, XXX–XXX

where V_{ecb} is the potential at equivalent CB position, ΔE_C the CB shift as estimated from Figure 7, and q the elementary charge. In Figure 8, the electron lifetime τ_n is plotted as a function of V_{ecb}. Upon SnO_2 NPs addition, $\log(\tau_n)$ linearly increases with V_{ecb}. Provided that the recombination kinetic constants remain unchanged and the amount of the electrons in TiO_2 CB is similar, the free I_3^- concentration in electrolyte will act as a key parameter in determining the recombination reaction in SnO_2-based DSCs. The same trend for τ_n was reconfirmed from open-circuit voltage decay (OCVD)[43,44] measurement in Figure S3 (Supporting Information). Therefore, it is claimed that the slow electron recombination is possible due to the lower amount of the free I_3^- concentration at the interface between the nanoporous TiO_2 and electrolyte. The reduction in the concentration of the free I_3^- inside the porous layer may be mostly due the adsorption of I_3^- on the acidic surface of SnO_2 incorporated to the electrolyte.

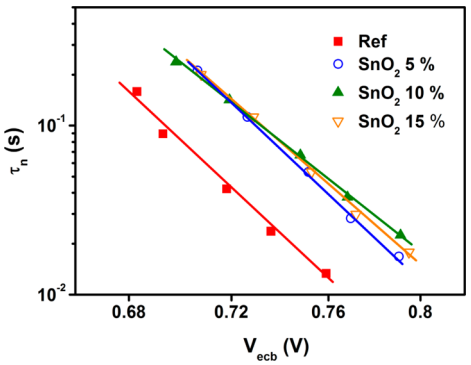

Figure 8. Electron lifetime (τ_n) as a function of potential (V_{ecb}) at equivalent CB position in DSCs upon the inclusion of SnO_2 NPs in polymer electrolytes.

Increase in J_{sc} upon SnO_2 Incorporation: IPCE Spectra. The short-circuit current density J_{sc} is calculated by integrating the incident photon to current conversion efficiency (IPCE) spectrum, which traces the quantum yield with respect to the exposed light wavelength.[45−47] The IPCE spectra are depicted in Figure 9a. The quantum yield overall increases in all DSCs incorporating SnO_2 NPs, and large improvement is observed between 350 and 450 nm.

The addition of SnO_2 up to 10 wt % resulted in the increment of the ionic conductivity mostly due to the increase in the diffusion coefficient of I_3^-. The higher ionic conductivity would make the diffusion limitation lower, as demonstrated by the photocurrent transient data (Figure 5), that is, the faster dye regeneration. Moreover, the SnO_2 addition in the electrolyte enables electron lifetimes to be elongated (Figure 8), improving the charge collection to the FTO side. As evidenced previously in Figure 2, SnO_2 NPs retain I_3^- to some extent, which diminishes the free ion concentration of I_3^-. The increased short-circuit current density J_{sc} may also have contribution from the lower light absorption by the intrapore electrolyte due to the lower I_3^- concentration in the TiO_2 pores. The fact that the larger IPCE increase is observed in the region at high wavelengths (350 and 450 nm) supports this hypothesis.

To evaluate a potential contribution to J_{sc} due to the light scattering effects, we assembled symmetrical cells consisting of transparent glasses filled with the PEO/PEGDME polymer electrolyte with or without 10 wt % SnO_2 NPs. The cells were spaced with 25 μm Surlyn after hot pressing. The reflectance results are depicted in Figure 9b. Similar reflectance is observed in both cases from 300 nm up to 450 nm, whereas at wavelengths larger than 550 nm scatter from SnO_2 NPs presents larger values than the probe sample. The results together with IPC data in Figure 9a suggest that the light scattering by SnO_2 NPs is negligible. The TiO_2 CB shift can also influence J_{sc}. For instance, the upward CB shift may lead to the decrease in both the electron injection efficiency and the electron diffusion rate, as previously reported.[37,38] In our case, we observed that only after 15 wt % addition of SnO_2 into the polymer electrolyte, the electron injection yield seems to be reduced with the consequent drop in the overall quantum yield.

As a result, it is suggested that the enhancement in the IPCE with SnO_2 NPs incorporated would be primarily due to the increase in the ionic conductivity and the decrease in I_3^- concentration inside the mesoporous film.

Charge-Transfer Resistance at the Pt-FTO/Electrolyte. Electrochemical impedance spectroscopy (EIS) is quite helpful to scrutinize the interfacial properties between counter electrode and electrolyte. Figure 10 shows the EIS results of a Pt−Pt symmetric cell measured in the frequency range of 1 MHz to 500 mHz at a bias voltage of 0 V under the dark condition. The first semicircle in the electrochemical impedance spectra obtained from the Pt−Pt symmetric cell is referred to as charge-transfer resistance (R_{ct}) at the Pt-FTO/electrolyte interface. In general, high R_{ct} hinders charge transfer from Pt counter electrode to electrolyte, consequently reducing the FF of DSCs. The EIS data indicate the decrease of R_{ct} with

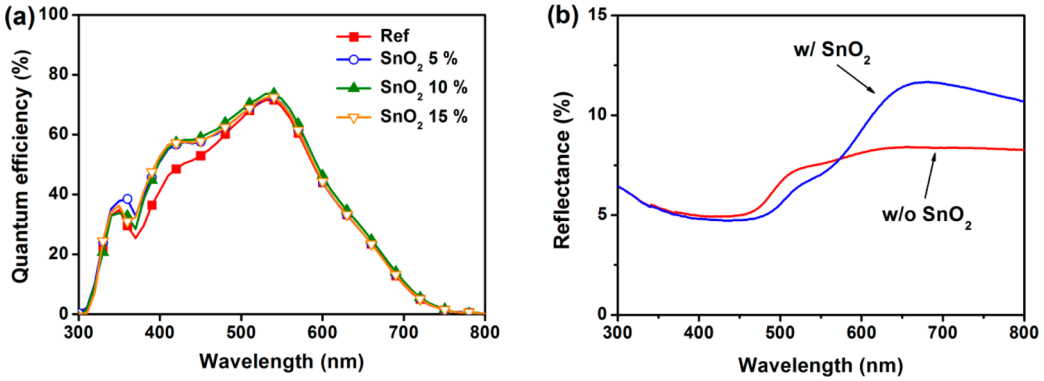

Figure 9. (a) Quantum efficiencies of the DSCs and (b) reflectance spectra of the polymer electrolytes with and without 10 wt % SnO_2 NPs in the wavelength range of 300−800 nm.

dx.doi.org/10.1021/jp4117485 | J. Phys. Chem. C XXXX, XXX, XXX−XXX

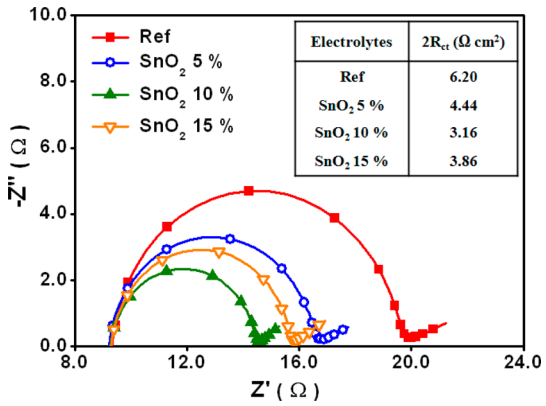

Figure 10. Impedance spectra of Pt−Pt symmetric cell measured at a bias voltage of 0 V and at an amplitude 10 mV in the dark condition. The frequency range was 1 MHz to 500 mHz. The charge transfer resistance (R_{ct}) is summarized in the inset table.

the addition of SnO_2 NPs (Figure 10). It is reasonable to think that the increased I_3^- concentration at the surface of the platinized counter electrode associated with faster I_3^- transport in the polymer electrolyte yields a lower R_{ct} at the Pt-FTO/electrolyte interface in DSCs. Also, specific interactions of Pt and SnO_2 NPs could help to increase charge transfer efficiency at this interface.

Substitution of SnO_2 NPs in the Polymer Electrolyte by TiO_2 NPs. To finish this work, we studied the results of adding TiO_2 NPs to the polymer electrolyte, which is more commonly used than SnO_2 NPs. Results summarized in Figure S5 and Table S1 in the Supporting Information showed no improvement in the performance of the DSCs built with electrolytes with TiO_2 NPs added. The adoption of SnO_2 NPs in the polymer electrolyte was much more fruitful in improving the overall power conversion efficiency of solid-state DSCs.

CONCLUSIONS

When SnO_2 nanoparticles were incorporated into the PEO/PEGDME polymer electrolyte, the overall power conversion efficiency of solid-state DCSs was improved to a large extent due to the increase in both V_{oc} and J_{sc} without sacrificing FF. The optimal contents of SnO_2 NPs were found to be 10 wt % after which performance of the cell started to decrease. The efficiency rise was attributable to an improvement in the physicochemical properties of the polymeric electrolyte after addition of the SnO_2 NPs. The strong Lewis acidity of the surface of SnO_2 NPs contributed to accumulation of a discrete anion-rich (I_3^-) layer over the surface SnO_2 NPs producing both a larger than 2-fold increase in the solid electrolyte conductivity and an improved contact with ethylene oxide units of PEO. At the same time, data indicate that concentrations of free I_3^- and K^+ ions inside the mesoporous film and therefore in the TiO_2 surface diminished, which is the origin of the improved V_{oc} through the observed rise of TiO_2 CB and decrease of recombination. The origin of J_{sc} was attributed to both the increase in the ionic conductivity and the lower competitive electrolyte light absorption by the electrolyte inside the pores of the TiO_2 film. The substitution of SnO_2 NPs by TiO_2 NPs produced no relevant changes with respect to the reference cells, which is attributable to the neutral effect in terms of acidity with respect to the dye-sensitized TiO_2 film

Therefore, it is believed that the effects of addition of SnO_2 NPs in the polymer electrolyte could also be considered to be a good avenue in designing high efficiency solid-state DSCs.

ASSOCIATED CONTENT

Supporting Information

Additional XRD patterns, work functions by UPS, electron diffusion by IMPS, electron lifetime by OCVD, and J−V performance of the TiO_2-NPs-based polymer electrolyte. This material is available free of charge via the Internet at http://pubs.acs.org.

AUTHOR INFORMATION

Corresponding Author

*E-mail: kangys@hanyang.ac.kr. Fax: +82-2-2296-2969. Tel.: +82-2-2220-2336.

Author Contributions

§H.C. and D.S. contributed equally to the research.

Notes

The authors declare no competing financial interest.

ACKNOWLEDGMENTS

This work was supported by a National Research Foundation of Korea (NRF) grant funded by the Korean government (MSIP) from the Center for Next Generation Dye-sensitized Solar Cells (no. 2013004800) and by the Korea Center for Artificial Photosynthesis (KCAP) (no. 2009-0093883). F.F.S. acknowledges financial support from Generalitat Valenciana under Project PROMETEO/2009/058.

REFERENCES

(1) O'Regan, B.; Grätzel, M. A Low-Cost, High-Efficiency Solar Cell Based on Dye-Sensitized Colloidal TiO_2 Films. *Nature* **1991**, *353*, 737−740.

(2) Yum, J.-H.; Baranoff, E.; Kessler, F.; Moehl, T.; Ahmad, S.; Bessho, T.; Marchioro, A.; Ghadiri, E.; Moser, J.-E.; Grätzel, M.; et al. A Cobalt Complex Redox Shuttle for Dye-Sensitized Solar Cells with High Open-Circuit Potentials. *Nat. Commun.* **2012**, *3*, 631−638.

(3) Yella, A.; Lee, H. W.; Tsao, H. N.; Yi, C.; Chandiran, A. K.; Nazeeruddin, M. K.; Diau, E. W. G.; Yeh, C. Y.; Zakeeruddin, S. M.; Grätzel, M. Porphyrin-Sensitized Solar Cells with Cobalt (II/III)-Based Redox Electrolyte Exceed 12 Percent Efficiency. *Science* **2011**, *334*, 629−634.

(4) Chung, I.; Lee, B.; He, J.; Chang, R. P. H.; Kanatzidis, M. G. All-Solid-State Dye-Sensitized Solar Cells with High Efficiency. *Nature* **2012**, *485*, 486−490.

(5) Bach, U.; Lupo, D.; Comte, P.; Moser, J. E.; Weissörtel, F.; Salbeck, J.; Spreitzer, H.; Grätzel, M. Solid-State Dye-Sensitized Mesoporous TiO_2 Solar Cells with High Photon-to-Electron Conversion Efficiencies. *Nature* **1998**, *395*, 583−585.

(6) Yang, L.; Xu, B.; Tian, H.; Boschloo, G.; Sun, L.; Hagfeldt, A.; Johansson, E. M. J. Initial Light Soaking Treatment Enables Hole Transport Material to Outperform Spiro-OMeTAD in Solid-State Dye-Sensitized Solar Cells. *J. Am. Chem. Soc.* **2013**, *135*, 7378−7385.

(7) Saito, Y.; Fukuri, N.; Senadeera, R.; Kitamura, T.; Wada, Y.; Yanagida, S. Solid State Dye Sensitized Solar Cells Using in Situ Polymerized PEDOTs as Hole Conductor. *Electrochem. Commun.* **2004**, *6*, 71−74.

(8) Tan, S.; Zhai, J.; Wan, M.; Meng, Q.; Li, Y.; Jiang, L.; Zhu, D. Influence of Small Molecules in Conducting Polyaniline on the Photovoltaic Properties of Solid-State Dye-Sensitized Solar Cells. *J. Phys. Chem. B* **2004**, *108*, 18693−18697.

(9) Kim, Y. J.; Kim, J. H.; Kang, M.-S.; Lee, M. J.; Won, J.; Lee, J. C.; Kang, Y. S. Supramolecular Electrolyte for Use in Highly Efficient Dye-Sensitized Solar Cells. *Adv. Mater.* **2004**, *16*, 1753−1757.

(10) Chen, C.-L.; Teng, H.; Lee, Y.-L. In Situ Gelation of Electrolytes for Highly Efficient Gel-State Dye-Sensitized Solar Cells. *Adv. Mater.* **2011**, *23*, 4199−4204.
(11) Lee, K. S.; Jun, Y.; Park, J. H. Controlled Dissolution of Polystyrene Nanobeads: Transition from Liquid Electrolyte to Gel Electrolyte. *Nano Lett.* **2012**, *12*, 2233−2237.
(12) Yu, Q.; Yu, C.; Guo, F.; Wang, J.; Jiao, S.; Gao, S.; Li, H.; Zhao, L. A Stable and Efficient Quasi-Solid-State Dye-Sensitized Solar Cell with A Low Molecular Weight Organic Gelator. *Energy Environ. Sci.* **2012**, *5*, 6151−6155.
(13) Chang, L.-Y.; Lee, C.-P.; Vittal, R.; Lin, J.-J.; Ho, K.-C. Enhanced Performance of a Dye-Sensitized Solar Cell with an Amphiphilic Polymer-Gelled Ionic Liquid Electrolyte. *J. Mater. Chem. A* **2013**, *1*, 3055−3060.
(14) Nogueira, A. F.; Durrant, J. R.; De Paoli, M. A. Dye-Sensitized Nanocrystalline Solar Cells Employing a Polymer Electrolyte. *Adv. Mater.* **2001**, *13*, 826−830.
(15) Wang, P.; Zakeeruddin, S. M.; Exnar, I.; Grätzel, M. High Efficiency Dye-Sensitized Nanocrystalline Solar Cells Based on Ionic Liquid Polymer Gel Electrolyte. *Chem. Commun.* **2002**, 2972−2973.
(16) Park, S.-H.; Lim, J.; Song, I. Y.; Lee, J.-R.; Park, T. Physically Stable Polymer-Membrane Electrolytes for Highly Efficient Solid-State Dye-Sensitized Solar Cells with Long-Term Stability. *Adv. Energy Mater.* **2013**, DOI: 10.1002/aenm.201300489.
(17) Wang, X.; Kulkarni, S. A.; Ito, B. I.; Batabyal, S. K.; Nonomura, K.; Wong, C. C.; Grätzel, M.; Mhaisalkar, S. G.; Uchida, S. Nanoclay Gelation Approach Toward Improved Dye-Sensitized Solar Cell Efficiencies: An Investigation of Charge Transport and Shift in the TiO_2 Conduction Band. *ACS Appl. Mater. Interfaces* **2013**, *5*, 444−450.
(18) de Freitas, J. N.; Nogueira, A. F.; De Paoli, M.-A. New Insights Into Dye-Sensitized Solar Cells with Polymer Electrolytes. *J. Mater. Chem.* **2009**, *19*, 5279−5294.
(19) Suzuki, K.; Yamaguchi, M.; Hotta, S.; Tanabe, N.; Yanagida, S. A New Alkyl-Imidazole Polymer Prepared as an Inonic Polymer Electrolyte by in Situ Polymerization of Dye Sensitized Solar Cells. *J. Photoch. Photobio. A* **2004**, *164*, 81−85.
(20) Nejati, S.; Lau, K. S. Pore Filling of Nanostructured Electrodes in Dye Sensitized Solar Cells by Initiated Chemical Vapor Deposition. *Nano Lett.* **2011**, *11*, 419−423.
(21) Kim, J. H.; Kang, M.-S.; Kim, Y. J.; Won, J.; Park, N.-G.; Kang, Y. S. Dye-Sensitized Nanocrystalline Solar Cells Based on Composite Polymer Electrolytes Containing Fumed Silica Nanoparticles. *Chem. Commun.* **2004**, 1662−1663.
(22) Kang, M.-S.; Kim, J. H.; Kim, Y. J.; Won, J.; Park, N.-G.; Kang, Y. S. Dye-Sensitized Solar Cells Based on Composite Solid Polymer Electrolytes. *Chem. Commun.* **2005**, 889−891.
(23) Kang, M.-S.; Kim, J. H.; Won, J.; Kang, Y. S. Oligomer Approaches for Solid-State Dye-Sensitized Solar Cells Employing Polymer Electrolytes. *J. Phys. Chem. C* **2007**, *111*, 5222−5228.
(24) Dey, A.; Karan, S.; De, S. Effect of Nanofillers on Thermal and Transport Properties of Potassium Iodide−Polyethylene Oxide Solid Polymer Electrolyte. *Solid State Commun.* **2009**, *149*, 1282−1287.
(25) Katsaros, G.; Stergiopoulos, T.; Arabatzis, I.; Papadokostaki, K.; Falaras, P. A Solvent-Free Composite Polymer/Inorganic Oxide Electrolyte for High Efficiency Solid-State Dye-Sensitized Solar Cells. *J. Photoch. Photobio. A* **2002**, *149*, 191−198.
(26) Stergiopoulos, T.; Arabatzis, I. M.; Katsaros, G.; Falaras, P. Binary Polyethylene Oxide/Titania Solid-State Redox Electrolyte for Highly Efficient Nanocrystalline TiO_2 Photoelectrochemical Cells. *Nano Lett.* **2002**, *2*, 1259−1261.
(27) Vrentas, J. S.; Duda, J. L. Diffusion in Polymer—Solvent Systems. I. Reexamination of the Free-Volume Theory. *J. Polym. Sci., Part B: Polym. Phys.* **1977**, *15*, 403−416.
(28) Nazmutdinova, G.; Sensfuss, S.; Schrödner, M.; Hinsch, A.; Sastrawan, R.; Gerhard, D.; Himmler, S.; Wasserscheid, P. Quasi-Solid State Polymer Electrolytes for Dye-Sensitized Solar Cells: Effect of the Electrolyte Components Variation on the Triiodide Ion Diffusion Properties and Charge-Transfer Resistance at Platinum Electrode. *Solid State Ionics* **2006**, *177*, 3141−3146.
(29) Zhou, Y.; Xiang, W.; Chen, S.; Fang, S.; Zhou, X.; Zhang, J.; Lin, Y. Quasi-Solid State Polymer Electrolytes for Dye-Sensitized Solar Cells: Effect of the Electrolyte Components Variation on the Triiodide Ion Diffusion Properties and Charge-Transfer Resistance at Platinum Electrode. *Chem. Commun.* **2009**, 3895−3897.
(30) Jeong, N. C.; Lee, J. S.; Tae, E. L.; Lee, Y. J.; Yoon, K. B. Acidity Scale for Metal Oxides and Sanderson's Electronegativities of Lanthanide Elements. *Angew. Chem., Int. Ed.* **2008**, *47*, 10128−10132.
(31) Ahn, H.-J.; Choi, H.-C.; Park, K.-W.; Kim, S.-B.; Sung, Y.-E. Investigation of the Structural and Electrochemical Properties of Size-Controlled SnO_2 Nanoparticles. *J. Phys. Chem. B* **2004**, *108*, 9815−9820.
(32) Kalaignan, G. P.; Kang, M. S.; Kang, Y. S. Effects of Compositions on Properties of PEO−KI−I_2 Salts Polymer Electrolytes for DSSC. *Solid State Ionics* **2006**, *177*, 1091−1097.
(33) Jing, G.; Zhen-Li, G.; Xiao-Li, Y.; Shu, G.; Zhong-Liang, Z.; Bo, W. Investigation of the Free Volume and Ionic Conducting Mechanism of Poly(ethylene oxide)-$LiClO_4$ Polymeric Electrolyte by Positron Annihilating Lifetime Spectroscopy. *Chin. Phys. B* **2012**, *21*, 107803.
(34) Yanagida, S. Recent Research Progress of Dye-Sensitized Solar Cells in Japan. *C. R. Chimie* **2006**, *9*, 597−604.
(35) Kontos, A.; Fardis, M.; Prodromidis, M.; Stergiopoulos, T.; Chatzivasiloglou, E.; Papavassiliou, G.; Falaras, P. Morphology, Ionic Diffusion and Applicability of Novel Polymer Gel Electrolytes with LiI/I_2. *Phys. Chem. Chem. Phys.* **2006**, *8*, 767−776.
(36) Suthanthiraraj, S. A.; Kumar, R.; Paul, B. J.; Mathew, V. Electrical Conductivity and Dielectric Behavior of PPG_4−$AgCF_3SO_3$:Al_2O_3 Nanocomposite Gel Polymer Electrolyte System. *J. Solid State Electr.* **2011**, *15*, 561−570.
(37) Boschloo, G.; Hagfeldt, A. Characteristics of the Iodide/Triiodide Redox Mediator in Dye-Sensitized Solar Cells. *Acc. Chem. Res.* **2009**, *42*, 1819−1826.
(38) Hamann, T. W.; Ondersma, J. W. Dye-Sensitized Solar Cell Redox Shuttles. *Energ. Environ. Sci.* **2011**, *4*, 370−381.
(39) Kopidakis, N.; Neale, N. R.; Frank, A. J. Effect of an Adsorbent on Recombination and Band-Edge Movement in Dye-Sensitized TiO_2 Solar Cells: Evidence for Surface Passivation. *J. Phys. Chem. B* **2006**, *110*, 12485−12489.
(40) Duffy, N. W.; Peter, L. M.; Rajapakse, R. M. G.; Wijayantha, K. G. U. A Novel Charge Extraction Method for the Study of Electron Transport and Interfacial Transfer in Dye Sensitised Nanocrystalline Solar Cells. *Electrochem. Commun.* **2000**, *2*, 658−662.
(41) Fabregat-Santiago, F.; Garcia-Belmonte, G.; Mora-Seró, I.; Bisquert, J. Characterization of Nanostructured Hybrid and Organic Solar Cells by Impedance Spectroscopy. *Phys. Chem. Chem. Phys.* **2011**, *13*, 9083−9118.
(42) Raga, S. R.; Barea, E. M.; Fabregat-Santiago, F. Analysis of the Origin of Open Circuit Voltage in Dye Solar Cells. *J. Phys. Chem. Lett.* **2012**, *3*, 1629−1634.
(43) Zaban, A.; Greenshtein, M.; Bisquert, J. Determination of the Electron Lifetime in Nanocrystalline Dye Solar Cells by Open-Circuit Voltage Decay Measurements. *ChemPhysChem* **2003**, *4*, 859−864.
(44) Bisquert, J.; Zaban, A.; Greenshtein, M.; Mora-Seró, I. Determination of Rate Constants for Charge Transfer and the Distribution of Semiconductor and Electrolyte Electronic Energy Levels in Dye-Sensitized Solar Cells by Open-Circuit Photovoltage Decay Method. *J. Am. Chem. Soc.* **2004**, *126*, 13550−13559.
(45) Tachibana, Y.; Hara, K.; Sayama, K.; Arakawa, H. Quantitative Analysis of Light-Harvesting Efficiency and Electron-Transfer Yield in Ruthenium-Dye-Sensitized Nanocrystalline TiO_2 Solar Cells. *Chem. Mater.* **2002**, *14*, 2527−2535.
(46) Hagfeldt, A.; Boschloo, G.; Sun, L.; Kloo, L.; Pettersson, H. Dye-Sensitized Solar Cells. *Chem. Rev.* **2010**, *110*, 6595−6663.
(47) Song, D.; Kang, M.-S.; Lee, Y.-G.; Cho, W.; Lee, J. H.; Son, T.; Lee, K. J.; Nagarajan, S.; Sudhagar, P.; Yum, J. H.; et al. Successful Demonstration of an Efficient $I^-/(SeCN)_2$ Redox Mediator for Dye-Sensitized Solar Cells. *Phys. Chem. Chem. Phys.* **2012**, *14*, 469−472.